JOURNAL OF MOLECULAR SPECTROSCOPY 114, 163–173 (1985)

Laser and Fourier Transform Spectroscopy of the $\tilde{A}^2\Pi$–$\tilde{X}^2\Sigma^+$ Transition of SrOH

C. R. BRAZIER[1] AND P. F. BERNATH[1]

Department of Chemistry, University of Arizona, Tucson, Arizona 85721

The combination of laser-induced fluorescence with Fourier transform spectroscopy has been used to analyze the 000-000 band of the $\tilde{A}^2\Pi$–$\tilde{X}^2\Sigma^+$ transition of SrOH. The rotational constants of both states have been determined. Relative intensities from the Fourier transform spectra provide information on rotational energy redistribution by collisions, and on the mixing of parallel character into the transition dipole moment.

I. INTRODUCTION

The visible bands of SrOH have been known for a very long time, the first observations being made by Herschel in 1823 (*1*). The carrier was not identified as SrOH until 1955, when James and Sugden (*2*) recognized the similarity with the bands of the isoelectronic strontium fluoride molecule. The bands of SrOH (as for all the alkaline earth metal hydroxides) are so badly overlapped that rotational analysis was not possible before the development of the tunable dye laser. The first such analyses were by Harris and co-workers (*3–6*). Other analyses of alkaline earth metal hydroxides have also been carried out by Bernath and co-workers (*7–9*).

We report here the analysis of the $\tilde{A}^2\Pi$–$\tilde{X}^2\Sigma^+$ system of SrOH which occurs in the region 6700–6900 Å, recorded by laser-induced fluorescence. The spectrum was initially measured using the technique of selective laser excitation with selective fluorescence detection to resolve the overlapped lines. To complete the analysis, Fourier transform spectra of laser-induced fluorescence were recorded using the McMath FTS at Kitt Peak National Observatory. As well as additional transition frequencies, these spectra provide important information on relative line intensities due to the simultaneous observation of all the lines. The relative line intensities are interpreted by inclusion of a parallel contribution to what is nominally a perpendicular transition dipole moment.

II. METHOD

The SrOH molecule was produced in a Broida-type oven (*10*). Strontium metal was resistively heated in an alumina crucible and the vapor was entrained in a flow of argon carrier gas. The metal atoms then reacted with a few mTorr of water added to the system. Significant amounts of SrOH could only be produced by increasing the

[1] Guest Investigator, National Solar Observatory, which is operated by the Association of Universities for Research in Astronomy, Inc., under contract with the National Science Foundation.

0022-2852/85 $3.00

total pressure to around 9 Torr. The direct bimolecular reaction to produce $\tilde{X}^2\Sigma^+$ SrOH, Sr(g) + $H_2O \rightarrow$ SrOH + H, is endothermic[2] by 0.8 eV (*11*); hence, this simple process is unlikely to contribute significantly. If, however, the Sr atoms are excited by pumping the $^3P_1$–^1S transition at 6892 Å with a laser, then the bimolecular reaction becomes exothermic by 1.0 eV. Experimentally, we find that SrOH can be produced at much lower pressure ($\simeq$1 Torr) and in typically 1000 times higher concentrations when the atomic line is excited.

The output of a Coherent 699-29 computer-controlled ring dye laser was focused vertically into the flame. Typical laser power was 200–500 mW using DCM dye pumped with 7 W of the 4880-Å line of a Coherent Innova 20 argon ion laser. The resultant SrOH fluorescence was dispersed through a 0.65-m monochromator and detected with a cooled photomultiplier tube with photon-counting electronics.

The spectra were recorded by scanning the dye laser and recording the fluorescence through the monochromator. By scanning the laser in the *P* branch and monitoring fluorescence from the connecting *R* branch, the complexity of the spectrum was much reduced (Fig. 2) (*12, 13*). This also made assignment easy, as transitions with a common excited state could be identified, and ground state combination differences were available (*4*).

Three channels of data were recorded simultaneously and displayed on the screen before storing on floppy disks. These consisted of the resolved fluorescence spectrum together with either the total undispersed signal or an iodine fluorescence spectrum, and 6-GHz Fabry–Perot fringes from the Coherent 699-29 wavemeter. The fringes were recorded only to provide a check on scan continuity. The wavemeter provides relative wavenumber measurements accurate to ± 0.002 cm^{-1}, but the iodine spectrum (*14*) was needed to maintain the absolute accuracy to this same standard. The data were corrected by subtracting 0.0056 cm^{-1} from the observed lines (*15*).

Two Doppler-limited Fourier transform spectra of SrOH, produced in a Broida oven, were also recorded. About 1 W of radiation from a Coherent 599-01 broadband dye laser (1-cm^{-1} bandwidth) was passed horizontally through the oven, and the resultant fluorescence was imaged onto the entrance aperture of the FT spectrometer. For one spectrum the laser was tuned to the $P_1 + Q_{12}$ bandhead and 13 scans were coadded in 1 $\frac{1}{2}$ hr. For the other the $^3P_1$–^1S Sr atomic line, which lies very near to the P_{12} branch bandhead (see Fig. 3), was excited. In this case 14 scans were coadded in 1 hr of observation. The resolution of the Fourier transform spectrometer was 0.020 cm^{-1}.

III. RESULTS AND DISCUSSION

A. Vibrational Structure

The $\tilde{A}^2\Pi$–$\tilde{X}^2\Sigma^+$ system was initially recorded by scanning the dye laser broadband (1-cm^{-1} linewidth) and monitoring the total fluorescence; this spectrum is shown in Fig. 1. The spin–orbit splitting for SrOH is 260 cm^{-1}, so that the $^2\Pi_{3/2}$ and $^2\Pi_{1/2}$ components are well separated and the $^2\Pi$ state conforms to Hund's case (a) coupling. Each of the subbands consists of six branches spaced approximately by $-3B$, $-B$, B,

[2] D_0^0(SrOH) = 92 kcal/mole [Ref. (*11*)].

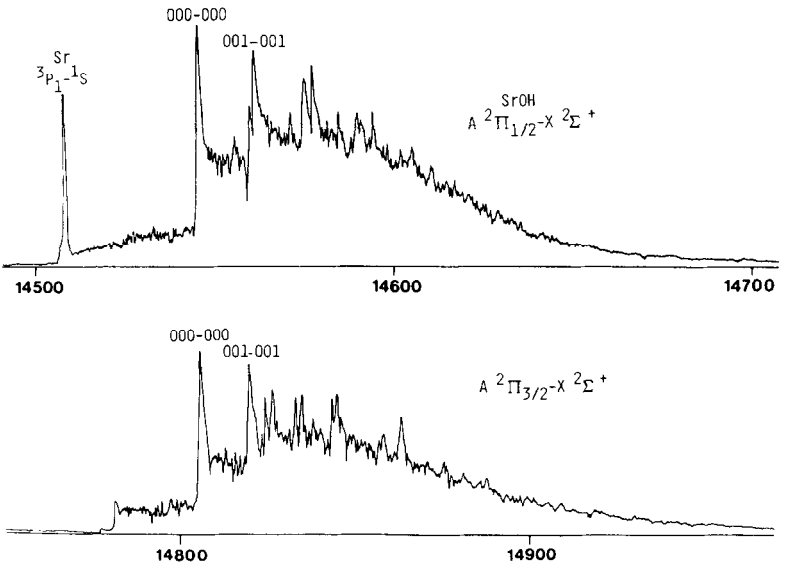

FIG. 1. The $\tilde{A}^2\Pi$–$\tilde{X}^2\Sigma^+$ system of SrOH recorded by scanning the dye laser (1-cm^{-1} bandwidth) and monitoring the total fluorescence. The approximate frequency scale is given in cm^{-1}.

$3B$, with the $-B$ and B branches doubled by the ground state spin–rotation interaction. The $-B$ branches reach bandheads at quite low J (20–30), giving rise to the prominent features in Fig. 1. The $-3B$ branches give rise to weak high-J bandheads ($\simeq$90), one of which can be seen at about 14780 cm^{-1}. Herzberg (*16*) provides notation, energy level diagrams, and a description of a case (a) $^2\Pi$–$^2\Sigma$ transition.

The transition involves promotion of an electron between two nonbonding metal-centered orbitals of Sr^+; this has little effect on the rest of the molecule. Thus the transitions which occur are highly diagonal and the small changes in vibrational frequencies cause the sequence structure to be badly overlapped. This is further complicated by the fact that two vibrations are of low frequency, Sr–O stretch at 522 cm^{-1} and the bend at 360 cm^{-1}, leading to population of many vibrational levels at 500 K.

The Q heads of the 000-000 vibrational band are easy to pick out as they are the most prominent features and lie at the low frequency side of each sequence. Some of the other features in Fig. 1 have been assigned on the basis of measured ground and excited state vibrational frequencies (Table I). These frequencies were measured by fixed frequency laser excitation and recording of the resolved fluorescence. A progression in the ground state Sr–O stretch is seen up to $\Delta v_3 = 3$. The excited state stretch (v'_3) was found to be 544 cm^{-1} from a laser excitation scan. Note that the labeling of the vibrations has been brought into conformity with customary spectroscopic practice (*17*): ν_1 is the O–H stretch, ν_2 is the Sr–O–H bend and ν_3 is the Sr–O stretch. Previous papers (*3–8*) had interchanged ν_1 and ν_3.

The bending vibration has Π character and hence the $\Delta v_2 = 1$ transition is formally forbidden (*18*). However, it is seen with about 1/8 the intensity of the 000-02^{0}0 transition. The $\tilde{A}^2\Pi$–$\tilde{X}^2\Sigma^+$ 000-010 transition is allowed by vibronic coupling. The $\tilde{A}^2\Pi$

TABLE I

SrOH Vibrational Frequencies (in cm^{-1}; estimated uncertainty ± 1 cm^{-1})

State	ν_2	$2\nu_2$	ν_3	$2\nu_3$	$3\nu_3$
$\tilde{X}^2\Sigma^+$	361	727	528	1048	1561
$\tilde{A}^2\Pi$	-	-	544	-	-

000 (Π) vibronic level interacts with the $\tilde{B}^2\Sigma^+$ 010 (Π) vibronic level so that the $\tilde{A}$–$\tilde{X}$ 000-010 transition appears by intensity borrowing. There is a definite trend in the observation of ν_2 in the alkaline earth metal hydroxides. For MgOH (*6*) and CaOH (*5, 7*) only the $\Delta v_2 = 2$ transition is seen. For SrOH the $\Delta v_2 = 1$ band is seen weakly while for BaOH (*9*) it is as strong as the $\Delta v_2 = 2$ transition. This increase in 000-010 band intensity correlates with the increase in spin–orbit coupling and is probably due to "spin–orbit vibronic" coupling (*19*). Fischer's discussion (*19*) of the spin–orbit vibronic coupling of singlet and triplet states in aromatic molecules is directly applicable with only a change in notation.

The spin–orbit Hamiltonian $[H_{SO}(q, Q)]$ is a function of both electronic (q) and vibrational (Q) coordinates, so the spin–orbit matrix element connecting Π and Σ vibronic states is

$$V_{SO}(Q) = \langle \Sigma | H_{SO}(q, Q) | \Pi \rangle \simeq V_{SO}(Q_0) + \sum_i \left(\frac{\partial V_{SO}}{\partial Q_i} \right)_{Q_0} Q_i,$$

where the integration is over electronic coordinates. Some manipulation (*19*) of $(\partial V_{SO}/\partial Q_i)_{Q_0}$ produces a term of the form

$$\sum_n \langle \Sigma | H_{SO} | n\Pi \rangle \left\langle n\Pi \left| \frac{\partial He}{\partial Q_i} \right| \Pi \right\rangle \Big/ (E_\Pi - E_{n\Pi})|_{Q_0},$$

which contains both spin–orbit mixing ($\langle \Sigma | H_{SO} | n\Pi \rangle$) and vibronic coupling ($\langle n\Pi | \partial He/\partial Q_i | \Pi \rangle$). The diagonal spin–orbit coupling constant of the $\tilde{A}^2\Pi$ state increases from 67 cm^{-1} in CaOH to 635 cm^{-1} in BaOH. Thus, the growing strength of the spin–orbit interaction is probably responsible for the increasing 000-010 band intensity.

B. Rotational Structure

The $\Delta B = -3$ and -1 branches of the 000-000 band were easily discernable, and the other branches were found by adjusting the monochromator to observe fluorescence in one of the known branches while scanning the dye laser. A monochromator bandpass of 1 Å was usually used for these measurements. All of the transitions were measured using the monochromator as a narrow-band filter to simplify the spectrum (*12, 13*). Ground state combination differences were obtained by reducing the bandpass to 0.2 Å, allowing fluorescence from only one rotational line to be detected; and, from these measurements, definite rotational assignments could be made. The FTS mea-

surements were made after the initial laser assignments had been completed so they were assigned by calculation.

The observed SrOH transition wavenumbers are listed in Table II. Only those lines which were used in the fit are given: low-J transitions with unresolved ground state spin–rotation splitting were not included. All the lines were weighted equally although some of the FTS measurements are of slightly lower accuracy. The average uncertainty as determined from the standard deviation of fit is 0.0025 cm^{-1}, which is consistent with the estimated measurement accuracy.

The observed transitions in Table II were fit to the $^2\Pi$ and $^2\Sigma^+$ energy level expressions of Zare *et al.* (*20*), using a nonlinear least-squares procedure. An explicit listing of these matrix elements can be found in Kotlar *et al.* (*21*). The molecular constants determined are given in Table III.

The ground state constants, while of higher precision, are in excellent agreement with those of Nakagawa *et al.* (*4*). It was found that the $^2\Pi$ state could be represented by only six constants (A, A_J, B, D, p, and q) and a transition energy. When additional higher-order terms such as H, p_D, and q_D were included, the quality of fit was only marginally improved, and these constants were not well determined; hence, they were excluded from the final fit.

The rotational constants B_0 and D_0 for the $\tilde{A}^2\Pi$ state are very similar to those for the $\tilde{B}^2\Sigma^+$ state (*6*). These two states form a unique perturber pair (*20*), with

$$\gamma_0 = -0.1667 \text{ cm}^{-1} \qquad \simeq p_0 \qquad = -0.1432 \text{ cm}^{-1}.$$

The pure precession value (*22*) is given by

$$p_0 \simeq \gamma_0 = \frac{2A_0B_0l(l+1)}{E(A^2\Pi - E(B^2\Sigma^+)}$$

$$= -0.157 \text{ cm}^{-1} \qquad \text{for} \qquad l = 1,$$

which is in reasonable agreement with the experimental results. If the expression is assumed to be exact, then an effective value for l may be calculated: this gives $l_{\text{eff}} = 0.96$. This does not imply that the $\tilde{A}$ and $\tilde{B}$ states are nearly pure p states. A similar estimate can also be made for the other lambda-doubling parameter, q;

$$q = \frac{2B_0^2l(l+1)}{E(A^2\Pi) - E(B^2\Sigma^+)}$$

$$= -1.51 \times 10^{-6} \text{ cm}^{-1} \qquad \text{for} \qquad l = 1.$$

Again this is in reasonable agreement with the experimental result of -1.91×10^{-4} cm^{-1}.

A prediction of the ground state microwave spectrum of SrOH can be made using the constants obtained together with the energy level expressions for $^2\Sigma$ states (*16*). The strong lines have $\Delta N = \Delta J$; these are given in Table IV for N'' up to 9. Each transition consists of a doublet split by 73 MHz due to the spin–rotation interaction.

The error estimates for the fitted constants imply a precision of between 0.5 MHz for the low-N transitions and 5 MHz for the high-N ones. Due to the possibility of systematic errors, the predictions are probably only accurate to about 10 MHz. This is consistent with the small systematic trends in the residuals of Table II.

TABLE II

Observed Transitions in Wavenumbers in the 000-000 Band of the $A^2\Pi$–$X^2\Sigma^+$ Transition of SrOH

J	$P_{12}(J)$	O-C[a]	$P_1(J)$	O-C	$Q_{12}(J)$	O-C	$Q_1(J)$	O-C	$R_{12}(J)$	O-C	$R_1(J)$	O-C
3.5	14539.5929	0.0029										
4.5	14538.8050	0.0028							14543.7270	-0.0021	14547.0736	0.0032
5.5	14538.0240	0.0009							14543.9642	0.0002		
6.5	14537.2555	0.0029					14543.9520	0.0037	14544.2001	-0.0075	14548.8261	-0.0017
7.5	14536.4940	0.0029					14544.1960	0.0066	14544.4550	-0.0049	14549.7179	-0.0014
8.5	14535.7390	0.0008					14544.4390	-0.0002	14544.7187	-0.0021	14550.6218	0.0023
9.5							14544.7001	0.0024	14544.9850	-0.0053	14551.5339	0.0056
10.5	14534.2608	0.0021					14544.9611	-0.0037			14552.4492	0.0036
11.5	14533.5343	0.0022					14545.2371	-0.0035	14545.5530	-0.0024	14553.3734	0.0019
12.5	14532.8156	0.0014					14545.5233	-0.0017	14545.8491	-0.0018	14554.3092	0.0033
13.5	14532.1066	0.0015					14545.8241	0.0060	14546.1509	-0.0042	14555.2558	0.0069
14.5	14531.4062	0.0013					14546.1150	-0.0049	14546.4721	0.0042	14556.2046	0.0041
15.5	14530.7163	0.0029					14546.4267	-0.0035	14546.7894	0.0000	14557.1632	0.0026
16.5	14530.0302	-0.0005					14546.7465	-0.0028	14547.1156	-0.0039	14558.1328	0.0037
17.5	14529.3648	-0.0021					14547.0798	0.0028	14547.4555	-0.0027	14559.1089	0.0027
18.5	14528.6942	0.0023					14547.4109	-0.0024	14547.7978	-0.0078	14560.0943	0.0024
19.5	14528.0383	0.0025					14547.7557	-0.0026	14548.1592	-0.0025	14561.0885	0.0025
20.5	14527.3909	0.0024					14548.1103	-0.0016	14548.5245	-0.0019	14562.0920	0.0034
21.5	14526.7522	0.0022					14548.4722	-0.0020	14548.8944	-0.0054	14563.1027	0.0031
22.5							14548.8452	0.0000	14549.2866	0.0048	14564.1228	0.0036
23.5							14549.2265	0.0018	14549.6643	-0.0081	14565.1521	0.0049
24.5					14540.8077	-0.0027	14549.6125	-0.0004	14550.0693	-0.0024	14566.1882	0.0045
25.5			14540.7469	-0.0016	14540.8523	-0.0035	14550.0086	-0.0012	14550.4767	-0.0029		
26.5			14540.7902	-0.0012	14540.9078	-0.0020	14550.4156	0.0003	14550.8946	-0.0016	14568.2838	0.0019
27.5			14540.8430	-0.0001	14540.9718	-0.0008	14550.8283	-0.0012	14551.3220	0.0006	14569.3455	0.0018
28.5			14540.9029	-0.0005	14541.0450	0.0009	14551.2515	-0.0008	14551.7470	-0.0083	14570.4175	0.0036
29.5			14540.9727	0.0002	14541.1257	0.0014	14551.6862	0.0025	14552.1973	-0.0005	14571.4961	0.0036
30.5			14541.0487	-0.0016			14552.1238	0.0000	14552.6507	0.0017	14572.5810	0.0014
31.5							14552.5723	-0.0002	14553.1075	-0.0013	14573.6776	0.0026
32.5	14520.3207	0.0058					14553.0275	-0.0024	14553.5766	-0.0006	14574.7821	0.0033
33.5	14519.7810	-0.0026	14541.3344	-0.0016	14541.5304	-0.0021	14553.4961	0.0002	14554.0527	-0.0016	14575.8942	0.0032
34.5	14519.2631	0.0019	14541.4463	-0.0024	14541.6544	-0.0019	14553.9689	-0.0016	14554.5355	-0.0045	14577.0128	0.0012
35.5	14518.7498	0.0019	14541.5681	-0.0021	14541.7878	-0.0011	14554.4542	0.0004	14555.0313	-0.0030	14578.1423	0.0018
36.5	14518.2459	0.0023	14541.6994	-0.0009	14541.9321	0.0018	14554.9451	-0.0006	14555.5326	-0.0048		
37.5	14517.7482	-0.0001	14541.8395	0.0002	14542.0775	-0.0029	14555.4448	-0.0015	14556.0512	0.0022		
38.5			14541.9875	0.0006	14542.2407	0.0015	14555.9541	-0.0014	14556.5647	-0.0046	14581.5800	0.0025
39.5	14516.7836	-0.0012	14542.1424	-0.0009			14556.4727	-0.0007	14557.0928	-0.0054	14582.7427	0.0029
40.5	14516.3130	-0.0037			14542.5812	-0.0019	14556.9987	-0.0012	14557.6323	-0.0035	14583.9121	0.0016
41.5	14515.8532	-0.0044	14542.4825	0.0001	14542.7679	-0.0003	14557.5319	-0.0031	14558.1870	0.0050	14585.0925	0.0031
42.5	14515.4075	-0.0001	14542.6641	-0.0009	14542.9614	-0.0006	14558.0767	-0.0021	14558.7399	0.0031	14586.2816	0.0049
43.5	14514.9620	-0.0047	14542.8571	0.0007	14543.1643	-0.0003	14558.6296	-0.0016	14559.2977	-0.0026	14587.4757	0.0033
44.5	14514.5289	-0.0059	14543.0565	-0.0001	14543.3767	0.0008	14559.1898	-0.0025	14559.8667	-0.0050	14588.6781	0.0018
45.5	14514.1181	0.0060	14543.2635	-0.0020			14559.7609	-0.0011	14560.4500	-0.0032	14589.8907	0.0022
46.5	14513.6995	0.0010					14560.3394	-0.0010	14561.0368	-0.0059	14591.1093	0.0004
47.5	14513.2901	-0.0039	14543.7101	0.0005	14544.0632	0.0006	14560.9326	0.0052			14592.3386	0.0009
48.5	14512.8955	-0.0032	14543.9448	-0.0001	14544.3084	-0.0006	14561.5236	0.0006			14593.5772	0.0025
49.5			14544.1875	-0.0014	14544.5650	0.0008					14594.8206	0.0006
50.5			14544.4418	0.0002	14544.8298	0.0016	14562.7378	-0.0024			14596.0759	0.0023
51.5			14544.7041	0.0009	14545.1045	0.0035					14597.3357	0.0004
52.5			14544.9760	0.0025	14545.3830	0.0005					14598.6060	0.0006
53.5			14545.2533	0.0006	14545.6743	0.0014					14599.8837	0.0001
54.5			14545.5407	0.0001	14545.9716	-0.0004					14601.1711	0.0010
55.5			14545.8385	0.0012							14602.4642	-0.0006
56.5											14603.7698	0.0020
57.5					14546.9224	0.0002					14605.0777	-0.0012
58.5			14546.7811	0.0009	14547.2574	0.0008					14606.3994	0.0012
59.5			14547.1137	0.0015							14607.7268	0.0010
60.5			14547.4523	-0.0006	14547.9500	-0.0017					14609.0617	0.0002
61.5			14547.8002	-0.0022	14548.3134	0.0009					14610.4063	0.0009
62.5			14548.1604	-0.0004	14548.6825	0.0004					14611.7571	-0.0003
63.5			14548.5255	-0.0025	14549.0593	-0.0013					14613.1178	0.0002
64.5			14548.9030	-0.0010							14614.4855	-0.0006
65.5			14549.2866	-0.0023	14549.8440	0.0000					14615.8617	-0.0009
66.5			14549.6822	-0.0003	14550.2494	0.0005					14617.2474	0.0002
67.5			14550.0847	-0.0004	14550.6620	-0.0007	14574.4883	0.0057	14575.4188	0.0013	14618.6384	-0.0017
68.5	14506.9275	-0.0004	14550.4951	-0.0013	14551.0869	0.0016	14575.2535	0.0023	14576.2009	0.0037	14620.0387	-0.0023
69.5	14506.7281	0.0011	14550.9166	-0.0000	14551.5159	-0.0009	14576.0312	0.0027	14576.9883	0.0028	14621.4478	-0.0023
70.5	14506.5364	0.0009	14551.3437	-0.0020	14551.9553	-0.0018	14576.8162	0.0019	14577.7840	0.0016	14622.8665	-0.0008
71.5	14506.3661	0.0027	14551.7807	-0.0029	14552.4052	-0.0011	14577.6110	0.0021	14578.5894	0.0013	14624.2884	-0.0042
72.5	14506.1817	0.0010	14552.2277	-0.0026	14552.8638	-0.0006	14578.4136	0.0015	14579.4041	0.0018	14625.7244	-0.0016
73.5	14506.0174	0.0000	14552.6843	-0.0017	14553.3300	-0.0013	14579.2260	0.0021	14580.2268	0.0015	14627.1658	-0.0017
74.5	14505.8661	0.0026	14553.1471	-0.0034	14553.8066	-0.0005	14580.0457	0.0012	14581.0585	0.0016		
75.5	14505.7210	0.0020	14553.6218	-0.0020	14554.2906	-0.0011	14580.8761	0.0025	14581.8985	0.0013		
76.5	14505.5878	0.0037	14554.1038	-0.0022			14581.7132	0.0017	14582.7468	0.0007		
77.5	14505.4612	0.0027					14582.5598	0.0018	14583.6053	0.0016		
78.5	14505.3465	0.0040					14583.4146	0.0015	14584.4671	-0.0028		
79.5	14505.2362	0.0003					14584.2772	0.0003	14585.3416	-0.0032		
80.5	14505.1384	-0.0004					14585.1496	0.0002	14586.2297	0.0013		
81.5	14505.0472	-0.0040					14586.0352	0.0046	14587.1163	-0.0043		
82.5	14504.9707	-0.0025					14586.9188	-0.0016	14588.0223	0.0007		
83.5	14504.9031	-0.0016					14587.8207	0.0018	14588.9296	-0.0015		
84.5	14504.8428	-0.0029					14588.7299	0.0039	14589.8525	0.0031		
85.5							14589.6340	-0.0078				
86.5							14590.5680	0.0016				

[a] Observed-Calculated in wavenumbers.

There is also the possibility of proton hyperfine structure; this has been discussed for CaOH (*8*). The effect is likely to be similar in SrOH, with splittings of a few MHz at low N dropping to zero at higher N where both rotational levels show the same hyperfine splitting.

TABLE II—*Continued*

J	$P_2(J)$	O-C	$P_{21}(J)$	O-C	$Q_2(J)$	O-C	$R_{21}(J)$	O-C
1.5							14807.3704	0.0013
2.5							14808.1504	0.0010
3.5								
4.5							14809.7375	-0.0012
5.5	14801.4760	0.0005					14810.5452	-0.0027
6.5	14800.7831	0.0006					14811.3659	-0.0007
7.5	14800.0979	-0.0012					14812.1936	-0.0014
8.5	14799.4254	-0.0001					14813.0308	-0.0023
9.5	14798.7603	-0.0013						
10.5	14798.1090	0.0016			14803.4380	-0.0037	14814.7376	-0.0004
11.5	14797.4618	-0.0012	14803.4176	0.0038	14803.3046	-0.0006	14815.6029	-0.0019
12.5	14796.8283	0.0000	14803.2776	0.0028	14803.1784	0.0000	14816.4788	-0.0024
13.5	14796.2064	0.0020	14803.1489	0.0031	14803.0608	-0.0005		
14.5	14795.5904	0.0022	14803.0279	0.0018	14802.9555	0.0015	14818.2591	-0.0037
15.5	14794.9873	0.0045	14802.9178	0.0015	14802.8587	0.0024	14819.1665	-0.0015
16.5	14794.3860	-0.0012	14802.8172	0.0009	14802.7689	0.0004	14820.0816	-0.0011
17.5	14793.8030	0.0016	14802.7268	0.0008	14802.6885	-0.0018	14821.0078	0.0008
18.5	14793.2251	-0.0002	14802.6416	-0.0038	14802.6211	-0.0008		
19.5	14792.6607	0.0017	14802.5689	-0.0057	14802.5641	0.0008	14822.8804	-0.0038
20.5	14792.1023	-0.0003	14802.5152	0.0017	14802.5161	0.0018		
21.5	14791.5608	0.0049	14802.4680	0.0058	14802.4768	0.0016	14824.8005	0.0009
22.5	14791.0204	0.0013	14802.4248	0.0042	14802.4429	-0.0029		
23.5	14790.4938	0.0017	14802.3862	-0.0025	14802.4243	-0.0018	14826.7524	-0.0006
24.5	14789.9748	-0.0001	14802.3644	-0.0023	14802.4183	0.0020	14827.7450	0.0010
25.5	14789.4669	-0.0006	14802.3564	0.0020	14802.4179	0.0018	14828.7444	-0.0001
26.5	14788.9682	-0.0018	14802.3537	0.0019	14802.4265	0.0007	14829.7566	0.0021
27.5	14788.4829	0.0005	14802.3592	0.0002	14802.4435	-0.0017	14830.7723	-0.0017
28.5	14788.0052	0.0007	14802.3751	-0.0009	14802.4737	-0.0007	14831.8039	0.0009
29.5	14787.5369	0.0003	14802.3990	-0.0038	14802.5142	0.0008	14832.8416	0.0002
30.5	14787.0785	0.0000	14802.4401	0.0007	14802.5631	0.0009	14833.8903	0.0009
31.5	14786.6305	0.0002	14802.4884	0.0026	14802.6191	-0.0017	14834.9481	0.0013
32.5	14786.1923	0.0004	14802.5416	-0.0003	14802.6846	-0.0045	14836.0130	-0.0006
33.5	14785.7650	0.0015	14802.6052	-0.0026	14802.7646	-0.0027	14837.0877	-0.0022
34.5	14785.3471	0.0022	14802.6818	-0.0018	14802.8546	-0.0007	14838.1738	-0.0018
35.5	14784.9370	0.0008	14802.7677	-0.0014	14802.9517	-0.0013	14839.2704	-0.0004
36.5	14784.5373	-0.0001	14802.8630	-0.0014	14803.0593	-0.0013	14840.3765	0.0011
37.5			14802.9665	-0.0031	14803.1755	-0.0025	14841.4885	-0.0010
38.5			14803.0828	-0.0017	14803.3035	-0.0017	14842.6127	-0.0002
39.5	14783.4011	0.0004	14803.2086	-0.0007	14803.4375	-0.0047	14843.7489	-0.0009
40.5	14783.0430	0.0014	14803.3388	-0.0051	14803.5844	-0.0047	14844.8892	0.0012
41.5	14782.6953	0.0029	14803.4836	-0.0047	14803.7464	0.0007	14846.0381	-0.0016
42.5	14782.3547	0.0015	14803.6426	0.0000	14803.9118	-0.0004	14847.1989	-0.0018
43.5	14782.0260	0.0020	14803.8043	-0.0023	14804.0860	-0.0026	14848.3703	-0.0009
44.5	14781.7077	0.0030	14803.9793	-0.0012	14804.2752	0.0004	14849.5507	-0.0003
45.5	14781.3982	0.0029	14804.1636	-0.0007	14804.4702	-0.0006	14850.7415	0.0014
46.5	14781.0972	0.0012	14804.3575	-0.0004	14804.6757	-0.0009	14851.9385	-0.0002
47.5	14780.8118	0.0052	14804.5621	0.0008	14804.8913	-0.0010	14853.1493	0.0028
48.5	14780.5282	0.0010	14804.7745	-0.0001	14805.1189	0.0010	14854.3630	-0.0008
49.5	14780.2597	0.0019	14804.9982	0.0005	14805.3548	0.0015	14855.5911	0.0007
50.5	14779.9995	0.0012	14805.2306	-0.0001	14805.5999	0.0013	14856.8239	-0.0024
51.5	14779.7499	0.0010	14805.4747	0.0011	14805.8555	0.0018	14858.0686	-0.0029
52.5	14779.5095	0.0000	14805.7254	-0.0009	14806.1187	-0.0000	14859.3266	0.0005
53.5	14779.2814	0.0013	14805.9909	0.0020	14806.3935	-0.0001	14860.5909	0.0010
54.5	14779.0601	-0.0006	14806.2611	-0.0002	14806.6781	-0.0002	14861.8630	-0.0001
55.5	14778.8541	0.0027	14806.5432	-0.0004	14806.9752	0.0022	14863.1481	0.0025
56.5	14778.6529	0.0008	14806.8345	-0.0013	14807.2787	0.0012	14864.4365	-0.0009
57.5	14778.4647	0.0019	14807.1391	0.0012	14807.5934	0.0016	14865.7412	0.0028
58.5	14778.2851	0.0025	14807.4520	0.0022	14807.9196	0.0035	14867.0493	0.0005
59.5	14778.1167	0.0023	14807.7732	0.0015	14808.2393	-0.0110	14868.3660	-0.0024
60.5	14777.9585	0.0032	14808.1009	-0.0025	14808.5940	-0.0003	14869.6986	0.0014
61.5	14777.8079	0.0017	14808.4449	-0.0002	14808.9465	-0.0018	14871.0352	-0.0002
62.5	14777.6672	-0.0000	14808.7952	-0.0014	14809.3119	-0.0002	14872.3828	0.0001
63.5	14777.5401	0.0017	14809.1583	0.0003	14809.6869	0.0010	14873.7393	-0.0001
64.5	14777.4232	0.0036	14809.5301	0.0007	14810.0672	-0.0024	14875.1051	-0.0001
65.5	14777.3163	0.0055	14809.9114	0.0008	14810.4657	0.0025	14876.4810	0.0007
66.5	14777.2170	0.0048	14810.3038	0.0020	14810.8664	-0.0003		
67.5	14777.1256	0.0019	14810.7018	-0.0010	14811.2785	-0.0016	14879.2588	0.0006
68.5			14811.1139	0.0001	14811.6984	-0.0050	14880.6628	0.0019
69.5	14776.9795	0.0024	14811.5335	-0.0012	14812.1337	-0.0030	14882.0735	0.0007
70.5	14776.9197	0.0008	14811.9617	-0.0039	14812.5782	-0.0017	14883.4956	0.0016
71.5			14812.4033	-0.0030	14813.0274	-0.0056	14884.9246	0.0003
72.5			14812.8532	-0.0038	14813.4949	-0.0012	14886.3639	0.0001
73.5			14813.3158	-0.0019	14813.9713	0.0022		
74.5			14813.7852	-0.0030				

The dipole moment of SrOH has not been measured. However, the dipole moment for the isoelectronic molecule SrF was found to be 3.47 D (*23*). The value for SrOH is likely to be smaller, probably around 2–3 Debye. The calculated frequencies will aid in a search for the microwave spectrum in either the laboratory or in extraterrestrial sources.

C. *Relative Intensities*

The first FT spectrum was recorded with excitation at the P_1, Q_{12} bandhead. The corresponding R_1 branch shows strong resonant lines between J of 10.5 and 32.5. The intensities of the P_{12}, Q_1, and R_{12} branches which originate from the other lambda-

TABLE III

Molecular Constants for the 000-000 Band of the $\tilde{A}^2\Pi$–$\tilde{X}\Sigma^+$ Transition of SrOH (in cm^{-1}; one standard deviation in parentheses)

Constant	$\tilde{X}^2\Sigma^+$ 000	$\tilde{A}^2\pi$ 000
T_0	0.0	14 674.332(2)
B_0	0.2492032(27)	0.2538873(27)
$D_0 X10^7$	2.1801(30)	2.1735(30)
$\gamma_0 X10^3$	2.4273(53)	-
P_0	-	-0.1432006(86)
$q_0 X10^4$	-	-2.0000(133)
A_0	-	263.51741(34)
$A_J X10^5$	-	7.0046(68)

doubling component (f) show a Boltzmann distribution ($T \simeq 500$ K) of population in the excited state f levels. The peak e/f population ratio is about 3/1, but the f levels could not have been populated directly by the laser. There is, however, no evidence of resonant ($\Delta J = 0$) transfer of population between the e and f levels since the distributions are different. However, the presence of a substantial Boltzmann population in the f component does suggest that the e and f levels communicate with each other.

The second FT spectrum was recorded with excitation of the $^3P_1$–$^1S_0$ Sr line at 6892 Å. There is no overlap of this line with the spectrum of SrOH. However, the P_{12} bandhead is only 0.4 cm^{-1} away so that it was excited by the 1-cm^{-1}-bandwidth dye laser. The lines with $J' = 83.5$–96.5 which could have been directly excited are not the strongest lines, however; instead, the maximum occurs at $J' = 71.5$, as can be seen in Fig. 3. The most reasonable explanation of this is that a partial relaxation of the population has occurred. In the limit of an infinite number of collisions, a Boltzmann

TABLE IV

Predicted Pure Rotational Transitions of SrOH (in MHz)

Transition N+1 ← N	Predicted Frequency F_1-F_1(e-e)	F_2-F_2(f-f)
1-0	14 979.	-
2-1	29 921.	29 846.
3-2	44 862.	44 787.
4-3	59 803.	59 728.
5-4	74 743.	74 669.
6-5	89 683.	89 608.
7-6	104 621.	104 547.
8-7	119 559.	119 484.
9-8	134 494.	134 420.
10-9	149 430.	149 355.

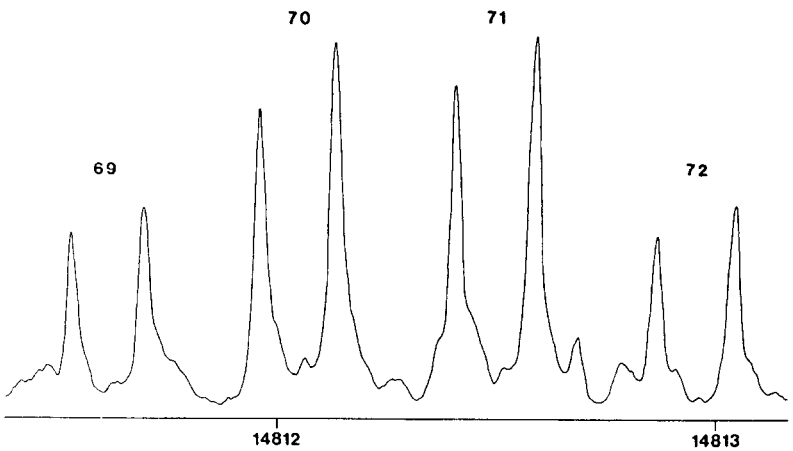

FIG. 2. A section of the Q_2 and P_{21} branches of SrOH recorded using resolved fluorescence detection. The numbers are N for the $^2\Sigma^+$ state, each transition being doubled by the ground state spin–rotation interaction.

distribution of population will occur. We appear to be looking at a situation part way between the fully relaxed and the initial laser-excited distributions. The high-J levels are well resolved in the Q_1 and R_{12} branches, shown in Fig. 4. The intensity of these transitions shows an additional maximum around $J = 88.5$ consistent with a small number of molecules emitting before undergoing collisions.

There is clear evidence in this spectrum of transfer to the e levels in the $^2\Pi$ state. In this case there is no strong Boltzmann background and the populations can be estimated fairly accurately, giving a value of 5:1 for the f:e ratio. The chance of a single

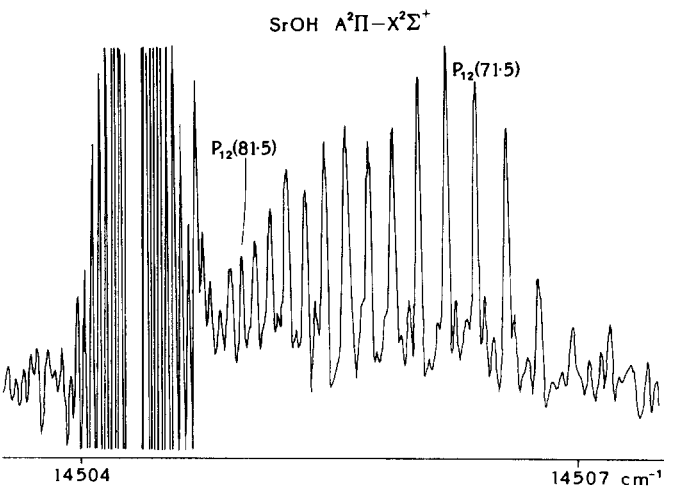

FIG. 3. Part of the Fourier transform spectrum of SrOH. Excitation is centered on the $^3P_1$–$^1S_0$ Sr atomic line, which is offscale by a factor of 100. The structure on this line is an instrumental artifact. At slightly higher frequency is seen the P_{12} bandhead, which is also excited by the laser. In addition there are several P_{12} lines which lie outside of the 1-cm^{-1} laser bandwidth.

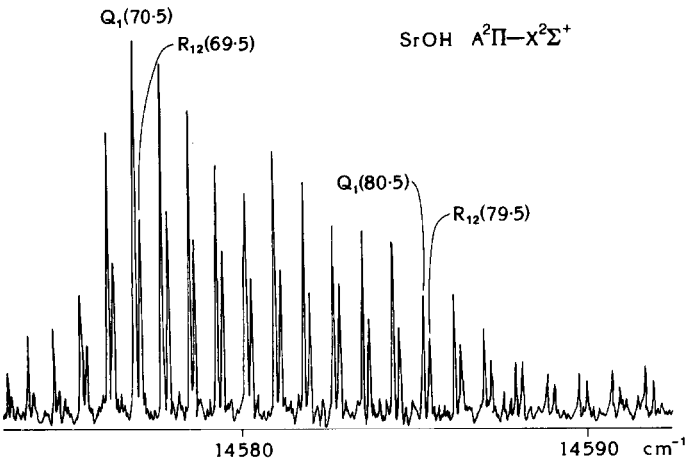

FIG. 4. A section of Fourier transform spectrum showing the Q_1 and R_{12} branches which originate from the same excited state rotational levels as shown in Fig. 3.

collision causing a change of parity must be less than this, however, as each molecule must have undergone several collisions at our pressure of 10 Torr before emitting.

There has been much interest recently in rotational energy transfer in $^2\Pi$ states of diatomic molecules (*24–26*), and this work represents the first observation of similar results in a triatomic species. The low propensity for e/f transfer is consistent with the qualitative explanation for other polar molecules given by Gottscho (*26*) and the quantitative work of Alexander (*24*).

It is also possible to make a comparison of the resonantly excited P_{12}, Q_1, and R_{12} branches. For a pure case a $^2\Pi$–$^2\Sigma^+$ transition these should have a 1:2:1 intensity ratio. If spin–uncoupling is included in the intensity calculations (*27*), then the ratio becomes 1:2.6:1. The measured ratio is 1:2.6:1.6; the difference is thought to arise from a parallel contribution to the formally perpendicular transition dipole moment. Expressions for the relative intensities of $\Omega = \frac{1}{2}$ states including this effect have been derived by Kopp and Hougen (*28*). Their expressions do not include spin–uncoupling, but as the ratio of P/R does not change due to uncoupling, an estimate of $\mu_{||}$ may be made from the relative intensities of these two branches. The calculation gives

$$\mu_\perp/\mu_{||} = 9.3.$$

This contribution arises from contamination of the $^2\Pi_{1/2}$ state by spin–orbit mixing $[A(L_-S_+ + L_+S_-)]$ with the $\tilde{B}^2\Sigma^+$ state. The wavefunction for the $\tilde{A}$ state acquires a proportion of $^2\Sigma$ character and $\mu_{||}$ can then make a contribution to the overall transition moment.

IV. CONCLUSION

The rotational analysis of the $\tilde{A}^2\Pi$–$\tilde{X}^2\Sigma^+$ system of SrOH has been performed by laser spectroscopic techniques. Laser-induced fluorescence from gas-phase free radicals has been detected by Fourier transform spectroscopy for the first time. The coupling of these two techniques gives the FT advantage of simultaneous recording of a large number of lines together with the simplification due to the selectivity of laser excitation.

ACKNOWLEDGMENTS

We thank Rob Hubbard for expert technical support during the Kitt Peak portion of this work. John Black kindly computed the intensities of a $^2\Pi$–$^2\Sigma$ transition for us. Acknowledgment is made to the donors of the Petroleum Research Fund, administered by the ACS, for partial support of this work. This research was also supported by the Research Corporation and the National Science Foundation (CHE-8306504).

RECEIVED: May 6, 1985

REFERENCES

1. J. F. W. HERSCHEL, *Trans. Roy. Soc. (Edinburgh)* **9,** 445–460 (1823).
2. C. G. JAMES AND T. M. SUGDEN, *Nature (London)* **175,** 333–334 (1955).
3. R. F. WORMSBECHER, M. TRKULA, C. MARTNER, R. E. PENN, AND D. O. HARRIS, *J. Mol. Spectrosc.* **97,** 29–36 (1983).
4. J. NAKAGAWA, R. F. WORMSBECHER, AND D. O. HARRIS, *J. Mol. Spectrosc.* **97,** 37–64 (1983).
5. R. C. HILBORN, ZHU QINGSHI, AND D. O. HARRIS, *J. Mol. Spectrosc.* **97,** 73–91 (1983).
6. YONG NI AND D. O. HARRIS, "The Structure of the Alkaline Earth Monohydroxides: MgOH and MgOD," in preparation.
7. P. F. BERNATH AND S. M. KINSEY-NIELSEN, *Chem. Phys. Lett.* **105,** 663–666 (1984).
8. P. F. BERNATH AND C. R. BRAZIER, *Astrophys. J.* **288,** 373–376 (1985).
9. S. M. KINSEY-NIELSEN, C. R. BRAZIER, AND P. F. BERNATH, "Rotational Analysis of the $\tilde{B}^2\Sigma^+$–$\tilde{X}^2\Sigma^+$ Transition of BaOH and BaOD," *J. Chem. Phys.*, accepted for publication.
10. J. B. WEST, R. S. BRADFORD, J. D. EVERSOLE, AND C. R. JONES, *Rev. Sci. Instrum.* **46,** 164–168 (1975).
11. E. MURAD, *J. Chem. Phys.* **75,** 4080–4085 (1981).
12. C. LINTON, *J. Mol. Spectrosc.* **69,** 351–364 (1978).
13. M. DULICK, P. F. BERNATH, AND R. W. FIELD, *Canad. J. Phys.* **58,** 703–712 (1980).
14. S. GERSTENKORN AND P. LUC, "Atlas du Spectre d'Absorption de la Molecule d'Iode," Laboratorie Amie-Cotton, CNRS 9145 Orsay, France.
15. S. GERSTENHORN AND P. LUC, *Rev. Phys. Appl.* **14,** 791–796 (1979).
16. G. HERZBERG, "Spectra of Diatomic Molecules," 2nd ed., p. 257, Van Nostrand-Reinhold, New York, 1950.
17. R. S. MULLIKEN, *J. Chem. Phys.* **23,** 1997–2011 (1955).
18. G. HERZBERG, "Electronic Spectra and Electronic Structure of Polyatomic Molecules," p. 152, Van Nostrand-Reinhold, New York, 1966.
19. G. FISCHER, "Vibronic Coupling," p. 136, Academic Press, New York, 1984.
20. R. N. ZARE, A. L. SCHMELTEKOPF, W. J. HARROP, AND D. L. ALBRITTON, *J. Mol. Spectrosc.* **46,** 37–66 (1970).
21. A. J. KOTLAR, R. W. FIELD, J. I. STEINFELD, AND J. A. COXON, *J. Mol. Spectrosc.* **80,** 86–108 (1980).
22. R. S. MULLIKEN AND A. CHRISTY, *Phys. Rev.* **38,** 87–119 (1931).
23. W. E. ERNST, J. KANDLER, S. KINDT, AND T. TORRING, *Chem. Phys. Lett.* **113,** 351–354 (1985).
24. M. H. ALEXANDER, *J. Chem. Phys.* **76,** 5974–5988 (1982).
25. O. NEDELEC AND J. DUFAYARD, *Chem. Phys.* **84,** 167–184 (1984).
26. R. A. GOTTSCHO, *Chem. Phys. Lett.* **81,** 66–69 (1981).
27. L. T. EARLS, *Phys. Rev.* **48,** 423–424 (1935).
28. I. KOPP AND J. T. HOUGEN, *Canad. J. Phys.* **45,** 2581–2596 (1967).